ACADEMIC PRESS

Available online at www.sciencedirect.com

SCIENCE DIRECT®

Journal of Computational Physics 186 (2003) 596–609

JOURNAL OF COMPUTATIONAL PHYSICS

www.elsevier.com/locate/jcp

Electric drill-string telemetry

José M. Carcione *, Flavio Poletto

Istituto Nazionale di Oceanografia e di Geofisica Sperimentale (OGS), Borgo Grotta Gigante 42C Sgonico, 34010 Trieste, Italy

Received 25 March 2002; received in revised form 20 January 2003; accepted 29 January 2003

Abstract

We design a numerical algorithm for simulation of low-frequency electric-signal transmission through a drill string. This is represented by a transmission line with varying geometrical and electromagnetic properties versus depth, depending on the characteristics of the drill-string/formation system. These properties are implicitly modeled by the series impedance and the shunt admittance of the transmission line. The differential equations are parabolic, since at low frequencies the wave field is diffusive. We use an explicit scheme for the solution of parabolic problems, based on a Chebyshev expansion of the evolution operator and the Fourier pseudospectral method to compute the spatial derivatives. The results are verified by comparison to analytical solutions obtained for the initial-value problem with a voltage source.

Keywords: Drill string; Voltage; Transmission line; Simulation; Low frequency

1. Introduction

Seismic-while-drilling technology has rapidly evolved during the last decade. An important application of the seismic telemetry method is the Seisbit^{R} technique, which uses the extensional wave generated at the drill bit (the pilot signals detected at the rig) to obtain RVSP seismograms [2]. Another possibility is to transmit information – from the bottom-hole-assembly (BHA) to the surface – through the drill string. This can be a key element in drill steering and prediction of lithology ahead-of-the-bit.

The transmission of electric pulses through the drill string has the advantage of instantaneous synchronization of seismic data. This problem has been studied since the 1970s [3,4,11,14,15,17,19,20] by means of analytical methods, which require the use of simplified models. High frequencies transmission, where displacement currents cannot be neglected, implies high transmission rates (high phase velocity), but also high attenuation [10]. On the other hand, at low frequencies, the attenuation is lower, but the data rates are lower [20]. Nevertheless, the electromagnetic system has higher data rates compared to more conventional systems, such as the mud-pulse method or the acoustic-telemetry method [9,12].

* Corresponding author. Tel.: +39-040-2140-345; fax: +39-040-327521.
E-mail address: jcarcione@ogs.trieste.it (J.M. Carcione).

0021-9991/03/$ - see front matter
doi:10.1016/S0021-9991(03)00085-8

Previous research demonstrated that for frequencies in the range 10–100 Hz the penetration is of the order of several kilometers. DeGauque and Grudzinski [11], using electromagnetic theory, show that because of the finite conductivity of the drill pipes, decreasing the frequency below a few hertz does not improve the communication. They demonstrate that the attenuation coefficient becomes a constant below a given frequency and that decreasing the frequency does not increase the communication range, but, on the contrary, decreases the transmission rate. They obtain an optimum frequency corresponding to a minimum attenuation and a maximal data rate. Xia and Chen [20] show that the frequency range of operation is essential, because high frequencies attenuate rapidly and very low frequencies are not suitable for transmission of information at a sufficient data rate.

Carcione and Poletto [10] have developed a theoretical and numerical approach for modeling electromagnetic wave propagation in drill strings. The model corresponds to a generalized telegrapher equation, which reduces to a diffusion – parabolic differential equation at low frequencies and to a hyperbolic (wave) equation at high frequencies. The method considers the presence of the coupling joints, non-uniform cross-section areas, and varying drill-string and formation electromagnetic properties. The formulation includes resistive and capacitive losses in the surrounding medium and drill string material. They have solved the high frequency differential equations by using a fourth-order Runge–Kutta method and the Fourier pseudospectral method to compute the spatial derivatives.

In this work, we develop a time-domain algorithm for the propagation of low-frequency electric signals along the drill-string. The algorithm uses an explicit scheme based on a Chebyshev expansion of the evolution operator and the Fourier pseudospectral method to compute the spatial derivatives [18]. This technique has spectral accuracy in time and space.

2. The electric-transmission system

2.1. The differential equations

Transmission of electric pulses through a drill string can be simulated by using the transmission line model developed by Carcione and Poletto [10]. The system, illustrated in Fig. 1, is governed by the following differential equations:

$$\frac{\partial^2 v}{\partial z^2} = \left(\frac{R}{\mathscr{R}} + \frac{\mathscr{C}}{C} + \frac{L}{\mathscr{L}}\right) v + \left(R\mathscr{C} + \frac{L}{\mathscr{R}}\right)\frac{\partial v}{\partial t} + L\mathscr{C}\frac{\partial^2 v}{\partial t^2} + \left(\frac{R}{\mathscr{L}} + \frac{1}{C\mathscr{R}}\right)\int v\,\mathrm{d}t + \frac{1}{C\mathscr{L}}\int\int v\,\mathrm{d}t\,\mathrm{d}t', \tag{1}$$

where as in the figure, ρ, ϵ and μ denote resistivity, permittivity and magnetic permeability, and the subindices f and d denote formation and drill string, respectively (see the figure). The series inductance and resistance, L and R, and shunt capacitance, $\mathscr{C}$, are measured by unit length, and the the series capacitance, C, and shunt resistance and inductance, $\mathscr{R}$ and $\mathscr{L}$, are measured per inverse of unit length (the inverse of $\mathscr{R}$ is the conductance per unit length). The circuit shown in Fig. 1(b) corresponds to a length δz of the line. The voltage and current are functions of depth z and time t, so that the terminal conditions are those shown in the figure, where v is the voltage and i is the electric current.

Eq. (1) contains time integrals, which are expensive to evaluate with numerical methods. Defining the new variables

$$q = \int i\mathrm{d}t \quad \text{and} \quad \varphi = \int v\,\mathrm{d}t, \tag{2}$$

the integrals are avoided, and the telemetry equations can be written in matrix form as

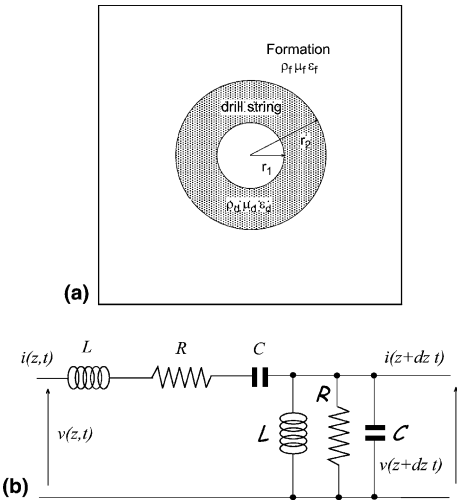

Fig. 1. Section of drill-string/formation system (a), and corresponding circuit representation (b): ρ, ϵ and μ denote resistivity, permittivity and magnetic permeability, respectively. The series- and shunt-inductance, capacitance and resistance, L, C, R and $\mathscr{L}$, $\mathscr{C}$, $\mathscr{R}$, characterize the system. The circuit corresponds to a length δz of transmission line. The voltage and current are functions of depth z and time t, so that the terminal conditions are those shown in (b), where v is the voltage and i is the current.

$$\frac{\partial}{\partial t}\begin{pmatrix} i \\ v \\ q \\ \varphi \end{pmatrix} = -\begin{pmatrix} RL^{-1} & L^{-1}\partial_z & (LC)^{-1} & 0 \\ \mathscr{C}^{-1}\partial_z & (\mathscr{R}\mathscr{C})^{-1} & 0 & (\mathscr{L}\mathscr{C})^{-1} \\ -1 & 0 & 0 & 0 \\ 0 & -1 & 0 & 0 \end{pmatrix}\begin{pmatrix} i \\ v \\ q \\ \varphi \end{pmatrix} + \begin{pmatrix} i_s \\ v_s \\ 0 \\ 0 \end{pmatrix}, \tag{3}$$

where ∂_z denotes spatial differentiation. We have introduced the source terms i_s and v_s.

The standard telegrapher equation is obtained for $C \to \infty$ and $\mathscr{L} \to \infty$ [16],

$$\frac{\partial^2 v}{\partial z^2} = \frac{R}{\mathscr{R}}v + \left(R\mathscr{C} + \frac{L}{\mathscr{R}}\right)\frac{\partial v}{\partial t} + L\mathscr{C}\frac{\partial^2 v}{\partial t^2}. \tag{4}$$

At low frequencies, the displacement currents can be neglected ($\mathscr{C} = 0$), and Eq. (4) can be written as a first-order differential equations in time,

$$\frac{\partial v}{\partial t} = \frac{\mathscr{R}}{L}\left(\frac{\partial^2}{\partial z^2} - \frac{R}{\mathscr{R}}\right)v + v_s, \tag{5}$$

where v_s is a source term.

2.2. Parameters of the drill-string formation system

The analysis of the resistances, inductances and capacitances as a function of the electromagnetic properties and geometrical characteristics of the drill string and formation, are given in [10]. We assume that the series capacitance of the drill pipes and coupling joints are infinite, and that a finite capacitance C arises at the contact between the joints and the pipes. Similarly, the shunt inductance $\mathscr{L}$ is introduced on heuristic grounds. Both the shunt capacitance and inductance are used here as free parameters and should be calculated or measured.

Summarizing, the field variables and material properties with the corresponding units in the SI system are

$$\begin{array}{ll} v\ [\mathrm{V}] & i\ [\mathrm{A}] \\ R=\rho_d/S\ [\Omega/\mathrm{m}] & \mathscr{R}=\rho_f\gamma\ [\Omega\cdot\mathrm{m}] \\ L=\mu_f\gamma\ [\mathrm{H}/\mathrm{m}] & \mathscr{L}\ [\mathrm{H}\cdot\mathrm{m}] \\ C\ [\mathrm{F}\cdot\mathrm{m}] & \mathscr{C}=\epsilon_f/\gamma\ [\mathrm{F}/\mathrm{m}], \end{array} \tag{6}$$

where

$$\gamma=\frac{1}{2\pi}\ln\left(\frac{2l}{r_2}\right), \tag{7}$$

where l is the drill-string length, r_1 and r_2 are the inner and outer radii, and $S=\pi(r_2^2-r_1^2)$ is the cross-section. (1 H = 1 V s/A, 1 F = 1 A s/V and 1 Ω = 1 V/A.) The free space permittivity and magnetic permeability are $\epsilon_0=8.85\times10^{-12}$ F/m and $\mu_0=4\pi10^{-7}$ H/m, respectively.

2.3. Phase velocity and attenuation factor

Let us assume a harmonic wave with a phase factor $\exp(\imath\omega t)$, where ω is the angular frequency and $\imath=\sqrt{-1}$. We define the series impedance and the shunt admittance as

$$Z=R+\imath\omega L+\frac{1}{\imath\omega C} \tag{8}$$

and

$$Y=\frac{1}{\mathscr{R}}+\imath\omega\mathscr{C}+\frac{1}{\imath\omega\mathscr{L}}, \tag{9}$$

respectively. Then, the phase velocity and attenuation factor are given by [10]

$$v_{\mathrm{p}}=-[\mathrm{Re}(s)]^{-1}\quad\text{and}\quad\alpha=\omega\,\mathrm{Im}(s), \tag{10}$$

respectively, where

$$s=\frac{\imath}{\omega}\sqrt{YZ} \tag{11}$$

is the complex slowness, and the operators "Re" and "Im" denote real and imaginary part.

3. The numerical algorithm

Eqs. (3) and (5) have the form

$$\frac{\partial\mathbf{w}}{\partial t}=\mathbf{G}\mathbf{w}+\mathbf{s}, \tag{12}$$

where $\mathbf{w}$ is the field vector, $\mathbf{s}$ is the source vector, and $\mathbf{G}$ is the propagation matrix containing the spatial derivatives and material properties. ($G=\partial^2/\partial z^2-R/\mathscr{R}$ in Eq. (5).)

We use the Fourier method [5,7,8,13], which consists of a spatial discretization and calculation of spatial derivatives using the fast Fourier transform. The Fourier method is a collocation technique in which a continuous function is approximated by a truncated series of trigonometric functions, wherein the spectral

(expansion) coefficients are chosen such that the approximate solution coincides with the exact solution at the discrete set of sampling or collocation points, The collocation points are defined by equidistant sampling points Since the expansion functions are periodic, the Fourier method is appropriate for problems with periodic boundary condition. In order to fulfill this condition, we model the ends of the string by adding grid points where the electrical resistivity is very high.

Considering a discretization with N number of grid points, the system (12) becomes a coupled system of $n \cdot N$ ordinary differential equations at the grid points, where n is the dimension of matrix $\mathbf{G}$. The solution to Eq. (12) subject to the initial condition $\mathbf{w}(0) = \mathbf{w}_0$ is formally given by

$$\mathbf{w}_N(t) = \exp(t\mathbf{G}_N)\mathbf{w}_N^0 + \int_0^t \exp(\tau\mathbf{G}_N)\mathbf{s}_N(t-\tau)\,\mathrm{d}\tau, \tag{13}$$

where $\mathbf{w}_N^0$ is the initial-condition field vector, $\exp(t\mathbf{G}_N)$ is called evolution operator, and the subindex N indicates that those quantities are discrete representation of the respective continuous quantities. We consider a separable source term $\mathbf{s} = \mathbf{a}_N h(t)$, where $\mathbf{a}_N$ is the spatial distribution of the source and the function $h(t)$ is the source time history. A fully discrete solution of (13) is achieved by approximating the evolution operator. For instance, if there is no source, the solution can expressed by

$$\mathbf{w}_N(t) = H_M(t\mathbf{G}_N)\mathbf{w}_N^0, \tag{14}$$

where H_M is a polynomial of degree M that converges to $\exp(t\mathbf{G}_N)$ in the domain that includes all the eigenvalues of the operator $t\mathbf{G}_N$.

To solve Eq. (13), we use a time-integration technique based on the Chebyshev expansion of the function $\exp(x)$ [18]. Let

$$y = \frac{1}{bt}(x + bt), \quad -1 \leqslant y \leqslant 1, \tag{15}$$

where b is the absolute value of the eigenvalue of matrix $\mathbf{G}_N$ having the largest negative real part (as we shall see later, the eigenvalues are close to the real axis and their real part is negative.) Using Eq. (15), we have

$$\exp(x) = \exp(-bt)\exp(bty) = \sum_{k=0}^{\infty} b_k T_k(y), \tag{16}$$

where $T_k(y)$ is the Chebyshev polynomial of order k [1], and

$$b_k = c_k \exp(-bt) I_k(bt) \tag{17}$$

for initial conditions without source, and

$$b_k = c_k \int_0^t \exp(-b\tau) I_k(b\tau) h(t-\tau)\,\mathrm{d}\tau \tag{18}$$

in the presence of source, without initial conditions,

$$c_k = \begin{cases} 1, & k = 0, \\ 2, & k \geqslant 1, \end{cases} \tag{19}$$

and I_k is the modified Bessel function of order k [1]. Thus, the M degree polynomial approximation of $\exp(x)$ is

$$H_M(x) = \sum_{k=0}^{M} b_k T_k(y(x)). \tag{20}$$

Because of (15), we substitute the operator $\mathbf{F}_N$ defined as

$$\mathbf{F}_N = \frac{1}{b}(\mathbf{G}_N + b\mathbf{I}) \tag{21}$$

for y, where $\mathbf{I}$ is the identity matrix. For instance, in the absence of sources, the fully discrete solution is

$$\mathbf{w}_N^M = \sum_{k=0}^{M} b_k T_k(\mathbf{F}_N)\mathbf{w}_N^0. \tag{22}$$

$T_k(\mathbf{F}_N)\mathbf{w}_N^0$ is computed by using the recurrence relation

$$T_k(u) = 2uT_{k-1}(u) - T_{k-2}(u), \quad k \geqslant 2, \tag{23}$$

$$T_0(u) = 1, \quad T_1(u) = u. \tag{24}$$

Hence,

$$T_k(\mathbf{F}_N)\mathbf{w}_N^0 = 2\mathbf{F}_N T_{k-1}(\mathbf{F}_N)\mathbf{w}_N^0 - T_{k-2}(\mathbf{F}_N)\mathbf{w}_N^0, \quad k \geqslant 2, \tag{25}$$

$$T_0(\mathbf{F}_N)\mathbf{w}_N^0 = \mathbf{w}_N^0, \quad T_1(\mathbf{F}_N)\mathbf{w}_N^0 = \mathbf{F}_N\mathbf{w}_N^0. \tag{26}$$

The algorithm is a three-level scheme, since it uses the recurrence relation. Accuracy and stability have been investigated by Tal-Ezer [18], who shows that the algorithm is much more efficient that a modified Euler scheme.

3.1. Example

Consider, for instance, the differential equation (5). The propagation matrix (in the continuum) is the scalar

$$G = \frac{\mathscr{R}}{L}\left(\frac{\partial^2}{\partial z^2} - \frac{R}{\mathscr{R}}\right). \tag{27}$$

In the Fourier method, the second derivative is replaced by $-k^2$, where k is the wavenumber. (Note that G takes real negative values.) The maximum wavenumber is the Nyquist wavenumber, which for a grid spacing dz is π/dz. Hence, the value of b corresponding to Eq. (5) is

$$b = \frac{\mathscr{R}}{L}\left(\frac{\pi^2}{dz^2} + \frac{R}{\mathscr{R}}\right). \tag{28}$$

As Tal-Ezer has shown [18], the polynomial degree M should be of the order of $\sqrt{bt}$ to obtain accurate solutions.

4. Analytical solutions

Analytical solutions are important to analyze the physics of the problem and verify the numerical algorithm. In this section, we obtain solutions of Eq. (5).

4.1. Voltage versus distance and frequency

Bhagwan and Trofimenkoff's solution [4] for a conducting string of finite length l is

$$v(l,\omega)=\frac{v_T Z_1}{(Z_1+Z_2)\cosh(\gamma_1 l)}, \tag{29}$$

where v_T is the input voltage,

$$Z_1=Z_{01}\coth(\gamma_1 l), \quad Z_2=Z_{02}\coth(\gamma_2\Delta l), \tag{30}$$

Δl is the length of a downhole electrode,

$$\gamma_1=\sqrt{\frac{R+\imath\omega L}{\mathscr{R}}}, \quad \gamma_2=\sqrt{\frac{R+\imath\omega L_2}{\mathscr{R}_2}}, \tag{31}$$

$$Z_{01}=\gamma_1\mathscr{R}, \quad Z_{02}=\gamma_2\mathscr{R}_2 \tag{32}$$

and

$$L_2=\frac{\mu_f}{2\pi}\ln\left(\frac{\Delta l}{r_2}\right), \quad \mathscr{R}_2=\frac{\rho_f}{2\pi}\ln\left(\frac{\Delta l}{r_2}\right). \tag{33}$$

Eq. (29) takes into account the boundary conditions at both ends of the string. The subindex 2 indicates properties of the downhole electrode.

The corresponding equation for an infinite rod or hollow cylinder is the differential equation (5). The phase velocity and attenuation factor can be obtained from (10) by setting $C=\infty$, $\mathscr{C}=0$ and $\mathscr{L}=\infty$ in Eqs. (8) and (9). In this case, the slowness (11) is simply

$$s=\frac{\imath\gamma_1}{\omega}. \tag{34}$$

The voltage associated with the infinite string is

$$v(l,\omega)=v_T\exp(-\alpha z). \tag{35}$$

In the limit as $l\to\infty$, Bhagwan and Trofimenkoff's solution (29) coincides with the solution of (5).

4.2. Time-domain solutions

We obtain transient solutions when initial conditions or source are prescribed.

4.2.1. Initial condition

The solution $v(z,t)$ of Eq. (5) for the initial condition $v(z,0)$ is given by

$$v(z,t)=v(z,0)*g(z,t), \tag{36}$$

where $*$ denotes spatial convolution and $g(z,t)$ is the Green's function. In the wavenumber domain, we have

$$v(k,t)=v(k,0)g(k,t), \tag{37}$$

where k is the real wavenumber, $v(k,0)$ is the spatial Fourier transform of the initial condition, and $g(k,t)$ is the Green's function (A.10). Substituting this equation into Eq. (37) yields

$$v(k,t) = v(k,0)H(t)\exp(-\mathscr{R}k^2 t/L)\exp(-Rt/L). \tag{38}$$

The effect of the first exponential on the right hand side is to filter the high wavenumbers.

We use as initial condition

$$v(z,0) = \exp\left[-\frac{\Delta k^2 (z-z_0)^2}{4}\right]\cos[\bar{k}(z-z_0)], \tag{39}$$

with a Gaussian shape in the wavenumber domain

$$v(k,0) = \frac{\sqrt{\pi}}{\Delta k}\left\{\exp\left[-\left(\frac{k+\bar{k}}{\Delta k}\right)^2\right] + \exp\left[-\left(\frac{k-\bar{k}}{\Delta k}\right)^2\right]\right\}\exp(-\imath k z_0), \tag{40}$$

where z_0 is the location of the peak , $\bar{k}$ is the central wavenumber, and $2\Delta k$ is the width of the pulse, such that $v(\bar{k}\pm\Delta k,0) = v(\bar{k},0)/e$.

The solution in the space domain $v(z,t)$ is obtained by a discrete inverse Fourier transform, using the fast Fourier transform.

4.2.2. Source

The solution $v(z,t)$ of Eq. (5) for zero initial conditions is given by

$$v(z,t) = v_s(t) * g(z,t), \tag{41}$$

where here $*$ denotes time convolution. In the frequency-domain, we have

$$v(z,\omega) = v_s(\omega)g(z,\omega), \tag{42}$$

where $v_s(\omega)$ is the time Fourier transform of the source, and $g(z,\omega)$ is the Green's function (A.6). The source pulse has the same form (39), replacing z by t and k by ω, where t_0 is a time delay, and $\bar{\omega}$ is the central frequency. The solution in the time domain $v(z,t)$ is obtained by a discrete inverse Fourier transform, using the fast Fourier transform.

5. Examples

The following are the parameters considered by Bhagwan and Trofimenkoff [4]: $l = 1000$ m, $r_1 = 0.02$ m, $r_2 = 0.025$ m, $\rho_d = 2.5\times10^{-7}\ \Omega\cdot$m, $\rho_f = 10\ \Omega\cdot$m, $\mu_f = \mu_0$ and $\Delta l = 5$ m. The phase velocity (a) and attenuation factor (b) versus frequency are shown in Fig. 2. Phase velocity and therefore data rates increase with frequency, but attenuation also increases.

Fig. 3 shows the normalized voltage (35) versus frequency at a distance $z = 1000$ m from the source. The dotted line is Bhagwan and Trofimenkoff's solution for a rod of finite dimensions ($l = 1000$ m).

Let us consider a drill-string system governed by Eq. (5) and the initial condition (39), with $\bar{k} = 0.02$ 1/m, $\Delta k = \bar{k}/2$, and $z_0 = 1650$ m. The properties of the system are given above, and R, $\mathscr{R}$, and L can be obtained from Eq. (6). We consider $N = 165$ grid points and a uniform grid spacing $dz = 20$ m. Fig. 4 shows a set of snapshots of the voltage at 1, 30, 60 and 90 ms. The dots represent the numerical solution and the solid line is the analytical solution (36).

Assume now the numerical algorithm when a source is introduced at $z_0 = 1659$ m. We consider $N = 165$ grid points and a grid spacing $dz = 20$ m. The source central frequency is $\bar{f} = 1000$ Hz, $\bar{\omega} = 2\pi\bar{f}$, $\Delta\omega = \bar{\omega}/2$ and $t_0 = 1.6$ ms. The low-frequency approximation neglects the displacement currents, i.e., the terms

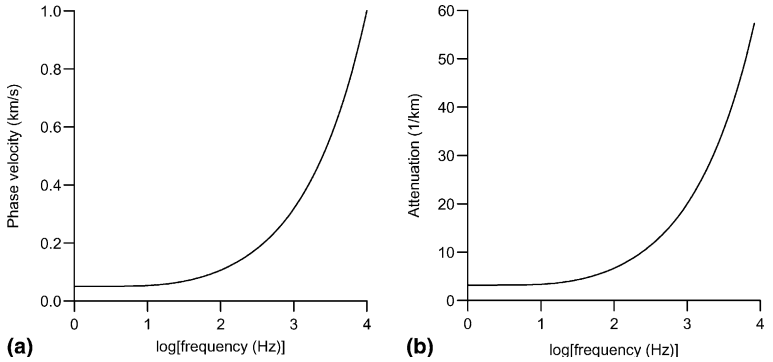

Fig. 2. Phase velocity (a) and attenuation (b) versus frequency. The drill-string parameters correspond to the example discussed by Bhagwan and Trofimenkoff [4].

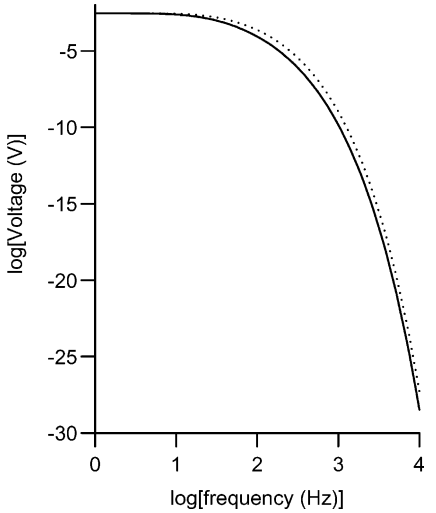

Fig. 3. Normalized voltage (35) versus frequency at a distance $z = 1000$ m from the source. The dotted line is Bhagwan and Trofimenkoff's solution for a rod of finite dimensions ($l = 1000$ m).

containing the shunt capacitance $\mathscr{C}$. For the standard telegrapher equation, this analysis can be performed in Eq. (11), in particular, considering the product YZ. This is given by

$$YZ = \left(\frac{1}{\mathscr{R}} + \imath\omega\mathscr{C}\right)(R + \imath\omega L) = \frac{R}{\mathscr{R}} + \imath\omega R\mathscr{C} + \imath\frac{\omega L}{\mathscr{R}} - \omega^2\mathscr{C}L. \tag{43}$$

At 1000 Hz, the relation between the absolute values of these four terms is $7.8 \times 10^{-3}/4.3 \times 10^{-8}/1/5.6 \times 10^{-6}$ $(1/\mathrm{m}^2)$, justifying the use of Eq. (5) to solve this problem. A snapshot of the voltage at 4 ms is shown in Fig. 5(a) (dots). The solid line is the analytical solution (41). This solution has been obtained with a discrete Fourier transform of 693 points and a time step of 0.05 ms. To compute successive snapshots, the snapshot shown in Fig. 5(a) is used as an initial condition. The voltage distribution at 20 ms is shown in Fig. 5(b) (dots), where the solid line represents the analytical solution.

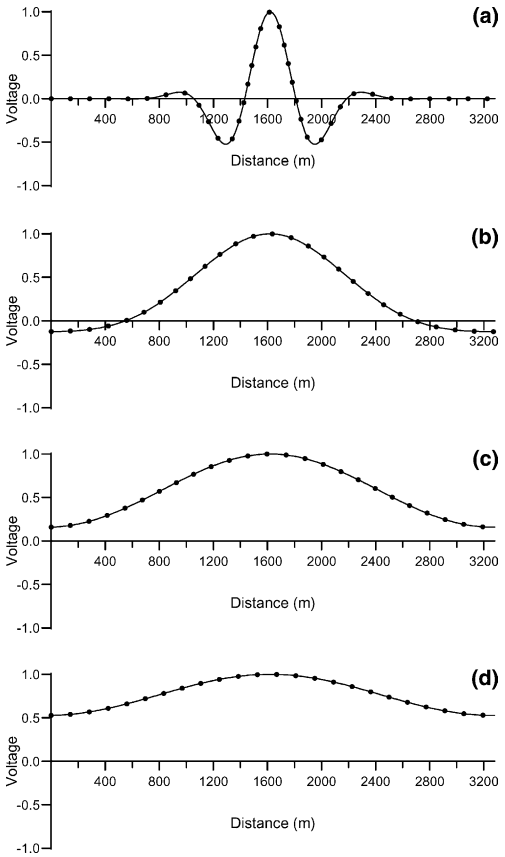

Fig. 4. Set of snapshots of the voltage at 1, 30, 60 and 90 ms. The dots represent the numerical solution and the solid line is the analytical solution (36). The amplitude ratio between snapshots, (a)/(b)/(c)/(d), is $1/2.6 \times 10^{-3}/1.4 \times 10^{-4}/9.6 \times 10^{-6}$.

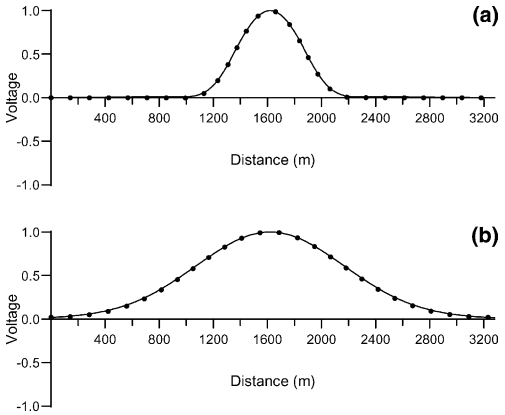

Fig. 5. Snapshot of the voltage at 4 ms generated by a source of 1000 Hz (a), and at 20 ms by considering (a) as an initial condition. The solid line represents the analytical solution. The amplitude ratio between snapshot (a) and (b) is 1/0.11.

In order to model the ends of the string, we consider a very high rod resistivity for the first and last 40 grid points of the mesh. Fig. 6 shows a snapshot of the voltage at 20 ms, generated by a source of 1000 Hz. The resistivity of the rod has been multiplied by 5000 between 0 and 800 m and between 2500 and 3280 m. There is no signal in those regions (compare to Fig. 5(b)).

The last example considers a drill string with the characteristics shown in Fig. 7. We use $N = 3465$ grid points and a uniform grid spacing $dz = 23$ cm. The source is located at grid point 1732 and has a central frequency of 1000 Hz. Each tool joint is modeled by two grid points and each pipe element by 37 grid points. The formation properties are $\rho_f = 2\ \Omega \cdot \mathrm{m}$ and $\mu_f = \mu_0$. Moreover, $\rho_d = 2.5 \times 10^{-7}\ \Omega \cdot \mathrm{m}$ for the pipes and $\rho_d = 250 \times 10^{-7}\ \Omega \cdot \mathrm{m}$ for the tool joints. This value describes a poor contact between pipe and tool joint rather than the resistivity of the tool joints, which is similar to that of the pipe.

Fig. 8(a) shows snapshots of the normalized voltage at 4 ms, with and without tool joints (solid and dashed lines, respectively). The attenuation is evident in the first case. Fig. 8(b) shows the voltage when the

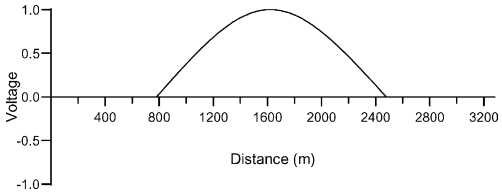

Fig. 6. Snapshot of the voltage at 20 ms generated by a source of 1000 Hz. The model is a finite rod of length 1700 m, extending from 800 to 2500 m.

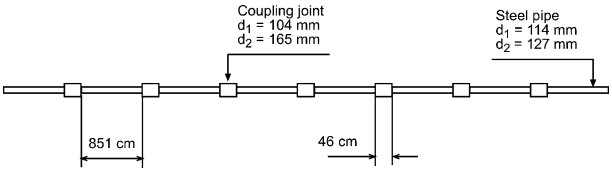

Fig. 7. Section of drill string consisting of pipes and tool joints (d_1 and d_2 denote the inner and outer diameters).

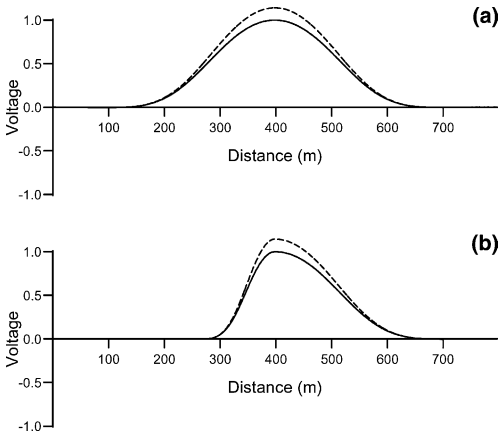

Fig. 8. (a) Snapshots of the normalized voltage at 4 ms, with and without tool joints (solid and dashed lines, respectively). (b) The voltage when the section $z < 400$ m is surrounded by a formation of lower resistivity.

section $z < 400$ m is surrounded by a formation of $\rho_f = 0.4\ \Omega \cdot \mathrm{m}$. As before the solid and dashed lines correspond to the rod and to the drill string, respectively. The lower shunt resistance implies higher attenuation of the voltage between 0 and 400 m.

6. Conclusions

We have developed a theoretical and numerical approach for modeling electromagnetic wave propagation in drill strings. The model corresponds to a generalized telegrapher equation, which reduces to a diffusion equation at low frequencies and to a hyperbolic (wave) equation at high frequencies. We have solved the diffusion equation including resistive losses in the surrounding medium and drill string material. Modeling at low frequencies requires an algorithm for parabolic differential equations. The algorithm is based on a Chebyshev expansion of the evolution operator. The use of this spectral method overcomes two drawbacks: low accuracy and stringent stability conditions, since the error in time decays exponentially.

In this phase of the research, we intend to obtain a physically meaningful theoretical and numerical model. Use of this theory for practical industrial application is a further matter of research, from the numerical and experimental points of view. Since the Fourier method is periodic, the model should be periodic or additional cells should be used at the extremes of the mesh to simulate periodicity. The boundary conditions are modeled by including regions of high resistivity at the ends of the string. In the example, these non-physical regions require the same grid points of the physical model. Since the modeling is one dimensional, this addition of grid points is not costly in terms of memory storage and computer time.

Other developments of the numerical code involve the inclusion of different media around the string (casing, cementation, etc.), and frequency effects of the series resistance of the rod and shunt capacitance of the formation. The series resistance can increase with frequency due to the skin effect ($R \propto \sqrt{\omega}$) and the presence of out-of-phase conduction currents, and the shunt capacitance must include dielectric losses in the formation.

Acknowledgements

Thanks to AGIP SpA for funding in part the research.

Appendix A. Green's functions

The Green's function $g(z,t)$ corresponding to Eq. (5) is the solution of

$$\frac{\partial g}{\partial t} = \frac{\mathscr{R}}{L}\left(\frac{\partial^2}{\partial z^2} - \frac{R}{\mathscr{R}}\right) g + \delta(z)\delta(t - t_0), \tag{A.1}$$

where δ denotes Dirac's function, and we have assumed a unit source located at $z = 0$ and activated at $t = t_0$. A double transform to the Laplace (Fourier) and wavenumber domains implies the substitution $\partial/\partial t \to p = \imath\omega$ and $\partial/\partial z \to -\imath k$, where ω is the angular frequency and k is the wavenumber. We obtain [6]

$$\tilde{\tilde{g}}(k,p) = \frac{\exp(-pt_0)}{p + \frac{1}{L}(k^2\mathscr{R} + R)}, \tag{A.2}$$

where a tilde denotes Fourier transform with respect to the spatial or temporal variables, and we have assumed zero initial conditions. The inverse Fourier transform to the space domain is

$$\tilde{g}(z,p) = \frac{L}{2\pi\mathscr{R}} \int_{-\infty}^{\infty} \frac{\exp(\imath kz - pt_0)\,\mathrm{d}k}{k^2 + \frac{1}{\mathscr{R}}(pL+R)}. \tag{A.3}$$

We use the residue theorem to solve this integral. The poles in the complex k-plane are

$$k_1 = \imath a, \;\; k_2 = -\imath a, \quad a(p) = \sqrt{\frac{pL+R}{\mathscr{R}}}. \tag{A.4}$$

For $z \geqslant 0$ we consider a counter-clockwise contour formed by the real k-axis and a half-circle including the pole k_1. The residue corresponding to this pole is

$$\frac{1}{2\imath a} \exp(-pt_0) \exp(-az). \tag{A.5}$$

Choosing the radius of the half-circle equal to ∞ and because the residue theorem states that the integral is equal to $2\pi\imath$ times the residue, we obtain

$$\tilde{g}(z,\omega) = \frac{L}{2a\mathscr{R}} \exp(-\imath\omega t_0) \exp(-az), \quad a(\omega) = \sqrt{\frac{\imath\omega L + R}{\mathscr{R}}}. \tag{A.6}$$

For $z < 0$ we consider a clockwise contour formed by the real k-axis and a half-circle including the pole k_2. The solution is given by (A.6), but substituting z by $-z$.

Let us assume the initial condition $v_0 = v(z,0) = \delta(z)$ and no sources. A double transform of (A.1) to the Laplace and wavenumber domains yields

$$\tilde{\tilde{g}}(k,p) = \frac{1}{p + \frac{1}{L}(k^2\mathscr{R} + R)}, \tag{A.7}$$

where we have used the property $\partial v/\partial t \to p\tilde{\tilde{g}} - \tilde{v}_0$, $\tilde{v}_0 = 1$.

To obtain $\tilde{g}(k,t)$, we compute the inverse Laplace transform of (A.7),

$$\tilde{g}(k,t) = \frac{1}{2\pi\imath} \int_{c-\imath\infty}^{c+\imath\infty} \frac{\exp(pt)\,\mathrm{d}s}{p + \frac{1}{L}(k^2\mathscr{R} + R)}, \tag{A.8}$$

where $c > 0$. There is one pole,

$$p_0 = -\frac{1}{L}(k^2\mathscr{R} + R). \tag{A.9}$$

Use of the residue theorem implies the Green's function

$$\tilde{g}(k,t) = H(t) \exp(p_0 t), \tag{A.10}$$

where $H(t)$ is the Heaviside function.

References

[1] M. Abramowitz, I.A. Stegun (Eds.), Handbook of Mathematical Functions, National Bureau of Standards, Applied Mathematical Series, 1964.
[2] L. Aleotti, F. Poletto, F. Miranda, P. Corubolo, F. Abramo, A. Craglietto, Seismic while-drilling technology: use and analysis of the drill-bit seismic source in a cross-hole survey, Geophys. Prosp. 47 (1999) 25–39.
[3] J. Bhagwan, F.N. Trofimenkoff, Electric drill stem telemetry, IEEE Trans. Geosci. Remote Sensing GE-20 (1982) 193–197.
[4] J. Bhagwan, F.N. Trofimenkoff, Drill stem resistance effects in electric telemetry links, IEEE Trans. Geosci. Remote Sensing GE-21 (1983) 141–144.

[5] J.P. Boyd, Chebyshev and Fourier Spectral Methods, Dover Pub., New York, 2001.
[6] R. Bracewell, The Fourier Transform and its Applications, McGraw-Hill Inc., New York, 1965.
[7] C. Canuto, M.Y. Hussaini, A. Quarteroni, T.A. Zang, in: Spectral Methods in Fluid Dynamics, Springer-Verlag, Berlin, 1987, pp. 7–10.
[8] J.M. Carcione, in: Wave Fields in Real Media: Wave Propagation in Anisotropic, Anelastic and Porous Media, Handbook of Geophysical Exploration, vol. 31, Pergamon Press Inc., New York, 2001.
[9] J.M. Carcione, F. Poletto, Simulation of stress waves in attenuating drill strings, including piezoelectric sources and sensors, J. Acoust. Soc. Am. 108 (2000) 53–64.
[10] J.M. Carcione, F. Poletto, A telegrapher equation for electric telemetering in drill strings, IEEE Trans. Geosci. Remote Sensing 40 (2002) 1047–1053.
[11] P. DeGauque, R. Grudzinski, Propagation of electromagnetic waves along a drill string of finite conductivity, SPE Drilling Eng. (1987) 127–134.
[12] D.S. Drumheller, S.D. Knudsen, The propagation of sound waves in drill strings, J. Acoust. Soc. Am. 97 (1995) 2116–2125.
[13] B. Fornberg, A Practical Guide to Pseudospectral Methods, Cambridge University Press, Cambridge, 1996.
[14] D.A. Hill, J.R. Wait, Electromagnetic basis of drill-rod telemetry, Electron. Lett. 14 (1978) 532–533.
[15] D.A. Hill, J.R. Wait, Calculated admittance of an idealized drill rod antenna in a lossy medium, IEEE Trans. Antennas Propagat. AP-23 (1979) 701–704.
[16] K.F. Sander, G.A.L. Reed, Transmission and Propagation of Electromagnetic Waves, Cambridge University Press, Cambridge, 1986.
[17] L. Soulier, M. Lemaitre, E.M. MWD data transmission status and perspectives, SPE/IADC 25686, 1993.
[18] H. Tal-Ezer, Spectral methods in time for parabolic problems, SIAM J. Numer. Anal. 26 (1989) 1–11.
[19] J.R. Wait, D.A. Hill, Theory of transmission of electromagnetic waves along a drill rod in conducting rock, IEEE Trans. Geosci. Electron. GE-17 (1979) 21–24.
[20] M.Y. Xia, Z.Y. Chen, Attenuation predictions at extremely low frequencies for measurement-while-drilling electromagnetic telemetry system, IEEE Trans. Geosci. Remote Sensing 31 (1993) 1222–1228.